Cross-section measurements for electron-H_3O^+ recombination*

R. A. Heppner, F. L. Walls,† W. T. Armstrong, and G. H. Dunn‡
Joint Institute for Laboratory Astrophysics, University of Colorado and National Bureau of Standards, Boulder, Colorado 80302
(Received 13 June 1974; revised manuscript received 2 September 1975)

Cross sections for electron-H_3O^+ recombination have been measured over an electron energy range of 0.060–1.15 eV by using a trapped-ion technique to contain an ion sample at a temperature of $\simeq 400$ K. The cross section deduced from these measurements can be represented by $\sigma = 4.6\times10^{-18}E^{-2.9}$ cm^2 for $0.038 < E \leq 0.110$ eV; $\sigma = 4.8\times10^{-16}E^{-0.79}$ cm^2 for $0.110 < E \leq 0.420$ eV; and $\sigma = 7.5\times10^{-17}E^{-2.9}$ cm^2 for $E > 0.420$ eV. Uncertainties are estimated to be at the $\pm 50\%$ level. Recombination-rate coefficients were calculated from the deduced cross sections, assuming a Maxwellian electron velocity distribution and trial forms for the cross section below 0.038 eV. Assuming the theoretical E^{-1} behavior for the cross section just above zero energy and comparing with the measured rate coefficient of Leu *et al.* at 540 K, we can deduce consistent cross sections below 0.038 eV to be $\sigma = 6.0\times10^{-15}E^{-1}$ cm^2 for $0 < E < 0.023$ eV, and $\sigma = 4.6\times10^{-18}E^{-2.9}$ cm^2 for $0.023 < E < 0.038$ eV. The calculated rate coefficients have temperature dependence $T_e^{-0.5}$ at 50 K and $T_e^{-1.43}$ at 10^5 K, and values of the coefficient are in good agreement with all direct measurements.

I. INTRODUCTION

Because of the almost universal presence of the water molecule, the hydronium ion (sometimes also called oxonium) H_3O^+ and its hydrates, $H_3O^+\cdot(H_2O)_n$, have been found to be important ions in many situations. These ions are found in significant amounts in the D region of the ionosphere,[1] and also appear to be the predominant ions in hydrogen or hydrocarbon flames.[2] The experimental work of Denes and Lowke[3] suggested that in modeling the characteristics of gas discharge lasers it might be important to consider the trace amounts of water vapor usually present in the gas mixtures. Indeed, modeling by Phelps[4] has indicated that the presence of H_3O^+ ions resulting from residual water vapor in laser discharges could explain many of the previously poorly understood phenomena associated with these discharges. In addition the hydronium ion was found to be one of the three major molecular ions in dense interstellar clouds in a model developed by Herbst and Klemperer.[5]

Recent calculations[6] show the ion to be of pyramidal structure, belonging to symmetry point group C_{3v}, and having an inversion barrier of about 0.15 eV. A static dipole moment[7] of about $0.4ea_0$ can be inferred from calculated[6] bond angles and interatomic distances. Rotational levels should be given approximately by $F(J,K) = 1.5\times10^{-3}J(J+1) - 7.6\times10^{-4}K^2$ eV. All normal modes of vibration are infrared active,[8] and the fundamentals observed[9] for ions trapped in crystal lattices ($\nu_2 \simeq 1100$ cm^{-1}, $\nu_4 \simeq 1700$ cm^{-1}, $\nu_1 \simeq 2600$ cm^{-1}, and $\nu_3 \simeq 3200$ cm^{-1}) are quite similar to those for NH_3 with which H_3O^+ is isoelectronic.

A principal mechanism for loss of H_3O^+ from plasmas is dissociative recombination of electrons and ions through reactions such as

$$e^- + H_3O^+ \rightarrow H_2O + H \rightarrow OH + H + H \text{ (or other neutral species)}. \quad (1)$$

To date there have been several determinations of the recombination rate coefficient,

$$\alpha = \int v f(v)\sigma(v)\,dv\,, \quad (2)$$

for electron–hydronium-ion recombination, where $\sigma(v)$ is the recombination cross section, and $f(v)$ is the electron velocity distribution (usually Maxwellian). These determinations include results from microwave afterglow measurements,[10] flame studies,[2,11-17] shock-tube experiments,[18] and glow discharge studies.[19] However, these rate-coefficient measurements have been over only a limited range of energies and some have been troubled by the presence or possible presence of other ion species.

We report recombination cross-section measurements on an isolated sample of H_3O^+ having an ion temperature of approximately 400 K over an electron energy range of $0.060 < E < 1.15$ eV. The rate-coefficient measurement of Leu *et al.*[10] at 540 K is then taken in complement with the measured cross sections and with predicted threshold forms for the cross section to deduce consistent cross sections at energies below 0.060 eV and to calculate rate coefficients from 10 to 1×10^5 K.

II. EXPERIMENTAL PROCEDURE

Cross sections were measured using the ion storage technique employed previously by Walls and Dunn.[20] Generally, in this method a stored sample of N_1 ions is bombarded for a time t by a beam of monoenergetic electrons of current i and energy E. At the end of t there remain only N_2 ions in the trap—some having been removed by recombination, and some by "natural decay processes" such as charge transfer, ion-atom interchange, diffusion, evaporation, etc. The cross section is then calculated from the expression

$$\sigma(E) = (e\mathfrak{A}/it)[\ln(N_1/N_2) - \ln(N_1'/N_2')] \ . \tag{3}$$

Here $\mathfrak{A}$ is a geometric quantity given by

$$\mathfrak{A} = \frac{2\pi \int \xi_i(r) r\, dr \int \mathfrak{F}(r) r\, dr}{\int \xi_i(r) \mathfrak{F}(r) r\, dr} \ , \tag{4}$$

where $\xi_i(r)$ is the radial density distribution of the ion cloud and $\mathfrak{F}(r)$ is the radial density distribution of the electron beam. In a simple picture $\mathfrak{A}$ is the area of the ion cloud as seen by the electron beam. The ratio N_1'/N_2' represents the ratio of ions before and after a period of *natural* decay only, i.e. with no electron beam.

A. Ion storage

The ions are stored in a Penning-style quadrupole ion trap[20-39] which is illustrated by the apparatus schematic in Fig. 1. The trap consists of three molybdenum electrodes, two end caps, and a central ring, constructed to be hyperboloids of revolution. A voltage V_0 applied to the ring gives rise to an electrostatic saddle potential in the trap given by $V = V_0(r^2 - 2Z^2)/(\rho^2 + 2d^2)$. Here $2\rho = 1.25$ cm is the equatorial diameter of the ring, $2d = 0.76$ cm is the axial distance between the end caps, and r and Z are cylindrical coordinates. The harmonic well thus created can contain or trap the ions along Z. However, ions also experience a repulsive force in the radial direction. Radial confinement of the ion sample is realized by use of a strong, uniform magnetic field along Z which induces cyclotron motion about the magnetic field lines, thus preventing any net radial motion.

Solutions[23,27] to the equations of motion for a trapped ion of charge q and mass M give

$$Z = Z_m \sin(\omega_z t + \delta) \tag{5}$$

and

$$\vec{r} = \vec{a}\, e^{\Omega_1 t} + \vec{b}\, e^{\Omega_2 t} \ , \tag{6}$$

where

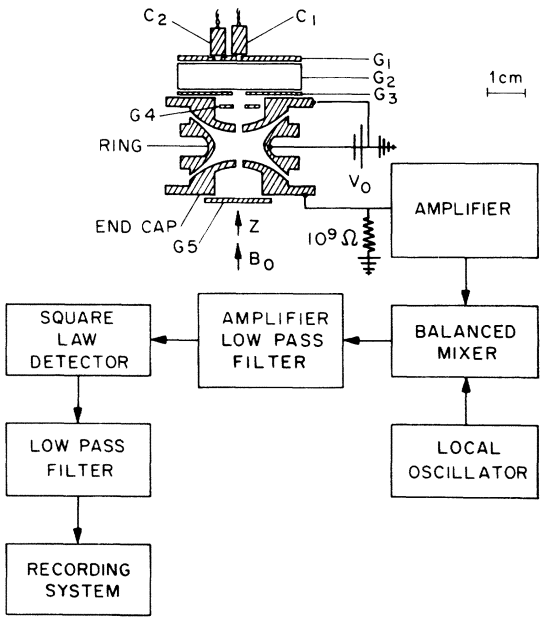

FIG. 1. Schematic diagram of the ion trap and associated equipment used in making recombination cross-section measurements.

$$\omega_z = \left(\frac{4qV_0/M}{\rho^2 + 2d^2}\right)^{1/2} \tag{7}$$

and

$$\Omega_{1,2} = i[\omega_c/2 \pm (\omega^2)^{1/2}] ,$$

defining

$$\omega_c = qB/M \tag{8}$$

and

$$\omega^2 = (\tfrac{1}{2}\omega_c)^2 - \tfrac{1}{2}\omega_z^2 . \tag{9}$$

If $\omega^2 < 0$ (i.e., $\omega_z^2 > \omega_c^2/2$), the solution for $\vec{r}$ is an exponentially growing spiral and there is no trapping. However, if $\omega^2 \geq 0$, then we have

$$\vec{r} = \vec{a}\exp[i(\omega_c/2 + |\omega|)t] + \vec{b}\exp[i(\omega_c/2 - |\omega|)t] \ . \tag{10}$$

Thus, the particle orbits on a circle of radius $|\vec{a}|$ with angular velocity $\omega_c' = \omega_c - \omega_m$, while the center of the circle precesses about the Z axis on a circle of radius $|\vec{b}|$ at the angular velocity $\omega_m = \omega_c/2 - \omega$. The three frequencies ω_z, ω_c, and ω_m are related by

$$2\omega_m^2 - 2\omega_m\omega_c + \omega_z^2 = 0 \ . \tag{11}$$

For a magnetic field of 1.17 T (1 Tesla = 10^4 G) and with $V_0 = 0.85$ V we have for H_3O^+ in our trap, $\nu_c' \sim 941$ kHz, $\nu_z \sim 80$ kHz, and $\nu_m \sim 3$ kHz.

Thus, ions in the trap with kinetic energies less than the well depth will be trapped for an indefinite time provided: (i) B is truly along the Z axis, (ii) the cyclotron radius is small compared to ρ, and (iii) $\omega^2 \geq 0$ (i.e., the radial magnetic force is larger than the radial electric force).

In practice there is not a perfect vacuum in the trap, and the ions may undergo ion-molecule reactions (charge transfer, ion-atom interchange, elastic collisions) with the ambient gas. If the rate coefficient for such reactions is β cm^3 sec^{-1}, then the ion population of a particular species will decay with a time constant $(\beta N_0)^{-1}$, where N_0 is the density of background molecules. A rate coefficient of 10^{-9} cm^3 sec^{-1} and a background pressure 1.3×10^{-8} Pa (1 pascal = 7.5×10^{-3} Torr) would lead to a lifetime against reaction of about 300 sec.

Ions are formed by electron bombardment of gas at ~450 K along the entire 0.76 cm distance between the end caps; and the resultant trapped ions then have a total energy ranging from the well depth (typically $0.4V_0$) to near zero. Thus, the initial translational energy distribution is characteristic of nearly uniform spatial distribution of ions along the harmonic well. Coulomb collisions establish a Maxwellian distribution of ion energies with a self-equilibration time given by Spitzer,[40]

$$\tau_{sc} = \frac{11.4A^{1/2}T^{3/2}}{nZ^4 \ln\Lambda} \text{ sec}, \tag{12}$$

where A is the molecular weight in amu, T is in K, n is ion density in cm^{-3}, Z is the charge multiplicity, and Λ is the ratio of a cutoff distance for the Coulomb potential to the impact parameter for scattering by $\frac{1}{2}\pi$. If we take the cutoff to be roughly the Debye shielding distance, and if $n = 10^6$, then $\ln\Lambda \simeq 12$; and τ_{sc} varies from about 500 msec at 2500 K to 22 msec at 300 K for $A = 19$.

As the distribution tends toward Maxwellian, some ions in the high-energy tail have more energy than the well depth. They escape, with the net effect of cooling the ion sample. Thus, the sample evaporatively cools in a short time to a temperature corresponding to about one-tenth the well depth.[27,29-31]

Cooling can also occur by radiative coupling of the ionic motion to the external circuit.[26,27,30,31,39] As the ions oscillate along Z, they induce image currents to flow between the end caps of the trap, and if the end caps are connected together with an effective resistance R_e, then Joule heating of the resistor exponentially damps the ions' motion with a time constant

$$\tau_R \simeq 8Md^2/q^2R_e. \tag{13}$$

The radiative coupling causes the ion temperature to approach that of the external circuit, which in this experiment is at about 300 K. For H_3O^+ ions where R_e is approximately 200 Ω, τ_R is approximately 6×10^5 sec. The collective motion of n ions is damped n times as fast.

Collisions between neutral-background-gas molecules and the trapped ions provide a third mechanism for cooling of the ion sample. By gently heating the sample with applications of the ω_z or ω_c frequencies, while the sample is trapped in a potential well deep enough to prevent evaporation, the time constant for combined radiative and collisional cooling can be measured. For H_3O^+ this time is approximately 150 sec and implies that the time constant for collisional cooling is approximately 150 sec since radiative cooling is so slow. This time can be compared with times calculated by using the measured mobilities of H_3O^+ in the presence of various gas species. For instance, H_3O^+ in H_2 at 4×10^{-8} Pa has a calculated equilibration time of 300 sec;[41] H_3O^+ in O_2 at the same pressure has a time of 150 sec.[42] It would be interesting to know the equilibration time for H_3O^+ in H_2O, since water vapor is the gas introduced to make the H_3O^+; however, no mobility measurements were available for this species. Because typical accomodation coefficients for molecules on surfaces are the order of 0.5,[43] the temperatures of the background gas within the trap will be the same as that of the trap—approximately 450 K under normal operating conditions. Thus the ion sample will approach not an equilibrium temperature of 300 K, but rather one determined by the relative contributions of the evaporative, radiative, and collisional mechanisms to the cooling process. For a typical sample of 10^4 H_3O^+ ions trapped with a potential $V_0 = 0.85$ V, the ion temperature is calculated to be approximately 400 K. This equilibrium temperature changes by +6% and −13% for 10^3 and 10^5 ions, respectively, because of the change in evaporative cooling rate with ion number. At a deeper well depth of 1.85 V the ion temperature stabilizes at approximately 440 K independent of the ion numbers used above, because of the lack of any evaporative cooling of the ion sample. A discussion of the effect of electron bombardment on the ion temperature will be considered in Sec. II C.

For $V_0 = 0.85$ V the cooled ions are then concentrated in about 2.4 mm along the Z axis. The potential varies about 0.018 V over this distance (corresponding to roughly $kT/2$). The ions then occupy a volume of roughly 0.02 cm^3 with a density of about 5×10^5 cm^{-3}.

In practice the system is evacuated to pressures the order of 1.3×10^{-8} Pa. Water vapor is introduced to a pressure of about 4×10^{-8} Pa, and with a $V_0 = 1.85$ V the H_2O is bombarded for a few min-

utes with 1 μA of 25-eV electrons. The gas inlet valve is then closed, and the target gas is pumped out with a time constant $\tau_V \approx 850$ sec. The ion sample stands for several minutes during which time H_3O^+ is formed through reactions such as

$$\begin{aligned} &H_2O^+ + H_2O \rightarrow H_3O^+ + OH \quad \text{(Ref. 44)} \\ &H_2O^+ + H_2 \rightarrow H_3O^+ + H \quad \text{(Ref. 45)} \\ &H_2O^+ + CH_4 \rightarrow H_3O^+ + CH_3 \quad \text{(Ref. 46)}. \end{aligned} \tag{14}$$

During this time the ions' kinetic degrees of freedom are cooled as described above, and the internal vibration and rotation degrees of freedom are primarily cooled by radiation (see discussion below), and collisions with background-gas molecules. Some hundreds of seconds after formation of the ions, V_0 is reduced to 0.85 V, and further cooling occurs during another subsequent wait of several hundred seconds. In the absence of any further perturbation (electrons, etc.) the ion number continues to decay primarily by reaction with the background gas of density ρ_b (effective rate coefficient β_b) and with the target gas of density $\rho_0 e^{-t/\tau_V}$ (rate coefficient β_t) according to the expression

$$\ln N = \ln N_0 - \beta_b \rho_b t + \beta_t \rho_0 \tau_V (e^{-t/\tau_V} - 1). \tag{15}$$

For our operating conditions the time for the H_3O^+ sample to decay to e^{-1} of its starting value is about 1500 sec. For $V_0 = 0.85$ V, a small evaporative loss of ions is also occurring during the natural decay period. However, evaporation accounts for less than 5% of the natural decay rate which is primarily due to ion-neutral reactions.

B. Detection and identification of ions

Trapped ions are detected by measuring the noise power in the image currents induced in the end caps of the trap. This is based on the scheme originally described by Dehmelt and Walls.[26,30] As indicated in Fig. 1, the signal present at one of the trap end caps is amplified, mixed with the output of a local oscillator at frequency ν, and put through a low-pass filter. Subsequent squaring of the mixer output enables us to measure the noise power present in the trap image currents at frequency ν. A peak in the noise power spectrum (with measured linewidth of typically 1 kHz) occurs when ν is equal to the ν_z of an ion species contained in the trap. The area under the peak is proportional to the product of the number of ions having the given q/M and their temperature. Once thermal equilibrium has been reached, this detection method provides a nondestructive means of measuring the number of ions of each species contained within the trap. The resonant peak occurs, of course, on a baseline of circuit noise. Peak-plus-background to background ratios range from 7 to 1, depending upon the number of ions in the trap and the bandwidth of the filter used.

Ion identification can be achieved by measuring the ν_z for resonance in the noise power spectrum and relating it to q/M by Eq. (7). However, mass identification with this method is good to only a few tenths of a mass unit without special effort. It is more convenient to apply a signal at ν_c' (near the cyclotron frequency). The accompanying heating of the ions at resonance is observed as an increase in the observed noise power, and q/M identification can be made to a few parts in 10^4. The mass of the ion under study in this experiment was measured by this means to be 19.02 ±0.02 amu; the mass of the hydronium ion is 19.018 amu. Coupled with consideration of the method of production, the identification of H_3O^+ is considered certain.

C. Bombardment with electrons

Electrons are introduced along the z axis of the trap from either of two electron guns shown schematically in Fig. 1. A conventional low-resolution electron gun composed of cathode C_1 and electrodes G_1 through G_4 provides a maximum usable current of approximately 1×10^{-7} A with FWHM of 120 meV. This gun is used to make ions by electron bombardment of the gas sample, and also provides recombination electrons at energies above 150 meV. A trochoidal design[47] high-resolution gun using cathode C_2 and the same electrodes G_1 through G_4 delivers a current of approximately 1×10^{-9} A with a FWHM of 40 meV, enabling recombination measurements to be performed at energies down to 50 meV. C_1 and C_2 are indirectly heated, impregnated cathodes. Electrodes G_1–G_5 are made of copper and have the following aperture sizes: G_1 has a circular aperture of 0.51 mm diam for the low-resolution gun, and a rectangular aperture 0.01 mm×1.52 mm for the high-resolution gun. G_2 consists of a set of parallel plates which provide the E field necessary for operation of the trochoidal monochromator; during low-resolution gun operation the parallel plates are tied to a common potential. Electrodes G_3 and G_4 have apertures of 2 mm diam, and proceeding in the direction of the electron beam, the two ion-trap end caps have rectangular apertures of 0.2 mm×2 mm and 0.3 mm×2.1 mm respectively. G_5 is the electron collector which is gold blacked. The entire trap assembly is enclosed in a cylindrical grounded electrostatic shield.

The electron collector G_5 is normally operated at about 7 V positive with respect to the end caps

in order to prevent reflected and secondary electrons from the gold black surface from reentering the trap area. Assuming diffuse scattering at the collector surface, and using the measured gold black collection efficiency of 75% for a primary electron energy of 7 V,[48,49] the fraction of the incident current energetically able to reenter the region of the trapped ion sample is 0.08% and 1.7% for recombination electron energies of 0.05 and 1.15 eV, respectively. These percentages represent upper limits, since we have assumed that any electrons not collected at the gold black surface have only been elastically reflected. If the uncollected electrons have lost any energy in their collision with the surface, the above percentages will be reduced. In any case, the effect of the reflected fraction will be negligible in comparison to the overall uncertainty in the recombination measurements.

Typical electron-energy distribution curves for the two electron guns are shown in Fig. 2. These distributions were obtained by a retarding potential measurement in which the potential of the electron gun was varied with respect to that of the central ring electrode.

Electrons in the magnetically confined beam have velocity components both parallel and perpendicular to the z axis. Energy associated with the transverse-velocity component is not measurable with the retarding potential method. However, a consideration of the sources[50] of the transverse velocities has led to estimated values of 50 meV and 10 meV for the transverse energy in the low- and high-resolution electron beams, respectively. Transverse velocities of the electrons also lead to spiral trajectories with an accompanying change in path length through the ion sample. The path-length changes have been evaluated following the discussion of Taylor *et al.*[50] In addition, electron energies are broadened and shifted by the 20-meV variation in potential over the region of the trap containing the ions. Data presented here have been corrected for these energy shifts and for path-length changes due to the spiraling motion.

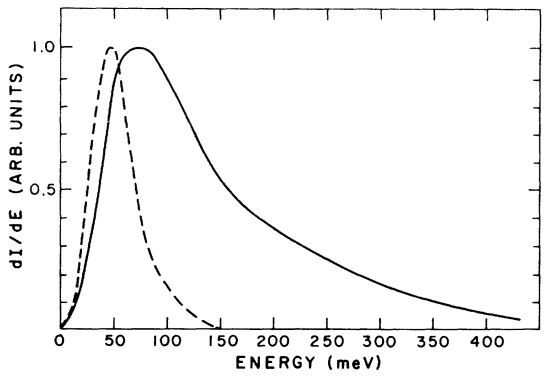

FIG. 2. Normalized electron energy distributions for the low- and high-resolution electron guns are represented by the solid and dashed lines respectively.

With electrons passing through the trap, the decay of ion number is given by

$$\dot{N} = -(i\sigma/e\mathfrak{A})N - \beta_b \rho_b N - \beta_t \rho_0 e^{-t/\tau_V} N - \xi_e . \quad (16)$$

The term ξ_e may include: (a) loss of ions due to space-charge distortion of the trap potential, (b) change in ion number due to heating of ions by energy transfer from the electron beam, (c) loss due to electron-ion collisions leading to dissociation or ionization, or (d) change in the first three terms on the right of Eq. (16) due to excitation of internal degrees of freedom of the ions or background gas. If ξ_e is negligible, the solution to Eq. (16) is given by Eq. (3), the expression used most often to determine cross sections from the measurements. There are, however, some conditions under which ξ_e contributes, and more complex analysis must be performed on the data.

Space charge due to the electron current produces a slight general depression of the harmonic potential well containing the ion sample. This depression has been calculated to be the order of 0.5 mV and 4 mV at typical operating conditions for the high- and low-resolution electron guns, respectively. The depression is a smooth function, and the well *distortion* will be an even smaller perturbation. To within the experimental uncertainty, the cross section was found to be independent of electron-gun current and thus space-charge density, as shown in Fig. 3. These data were taken with the low-resolution electron gun at 565 meV electron energy. The recombination data presented in Sec. III were taken with low-resolution gun currents in the low-middle part of the current range shown in Fig. 3; the high-resolution gun currents were 20 times smaller. We thus conclude that the contribution to ξ_e from space-charge effects is negligible.

When electrons pass through the ion sample, there are two possible mechanisms by which heating of the sample by the electron beam could occur: (i) a beam-plasma type of interaction resulting in collective motion of the ions, and (ii) an energy transfer from electron to ions through elastic binary collisions. For either mechanism, sufficient heating could affect cross-section measurements if the ion temperature increased to a degree where there was a significant evaporative loss of ions from the trap. We find no evidence for the existence of beam-plasma interaction such as a dramatic increase in signal due to center-of-

mass motion. This is reasonable because the Debye length for the trapped ions is approximately 0.13 cm, nearly as large as the dimensions of the sample, thus preventing the buildup of any electron-beam-induced collective motion of the sample.

Energy transfer through binary collisions between electrons and ions is a process which will occur. To determine whether the temperature of the ion sample will be affected by this additional source of energy, we have developed a mathematical model which predicts the number of ions $N(t)$ and their temperature $T(t)$ as functions of time. To obtain $N(t)$ and $T(t)$, we perform a numerical solution of two coupled differential equations:

$$\frac{dT}{dt} = -\frac{G(V_0, T)}{\tau_{sc}} - \frac{T-300}{\tau_r} - \frac{T-450}{\tau_c} + \frac{it_0}{1.5Nke}\langle \Delta E(N, T)\rangle , \tag{17a}$$

$$\frac{dN}{dt} = -\frac{H(V_0, T)}{\tau_{sc}} - \frac{N}{\tau_{rc}} - \beta_b \rho_b N - \beta_t \rho_0 e^{-t/\tau_v} N . \tag{17b}$$

The first term in Eq. (17a) represents the cooling effect due to the evaporation of ions from the finite potential well. It depends strongly upon the applied potential V_0 and the ion temperature T. The second and third terms account for radiative and collisional cooling of the ion sample. The last term describes the rate of increase of ion temperature due to energy input from Coulomb ion-electron collisions. The rate of energy decrease of an electron passing through an ion sample and thus the rate of energy increase of the ion sample can be obtained from Spitzer[40] as the quantity $\langle \Delta E \rangle$. The transit time of an electron through the ion cloud is given by t_0, and i is the electron current. In Eq. (17b) the first term represents the evaporative loss of ions from the trap, the second, third, and fourth terms describe loss of ions due to recombination and natural decay from ion–neutral-gas processes, respectively. Note that besides the explicit coupling between the two equations, the self-collision time τ_{sc} also depends upon $N(t)$ and $T(t)$.

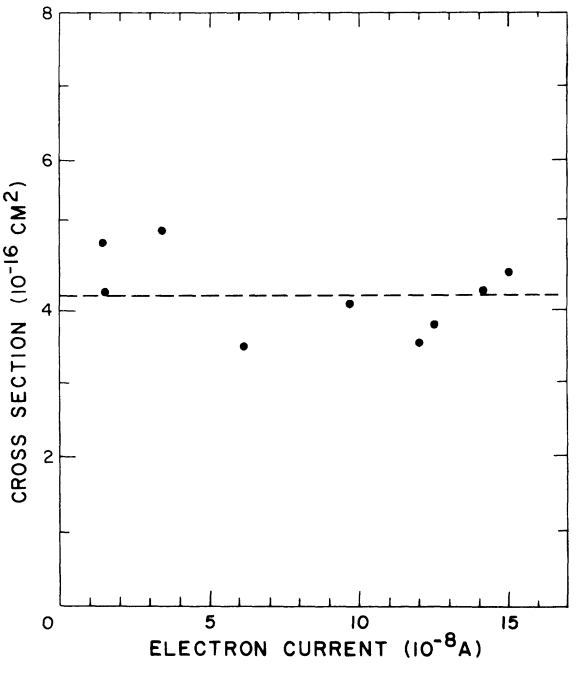

FIG. 3. Measured cross section at 565 meV as a function of electron current; data were taken using the low-resolution electron gun. Dots represent individual measurements, and the dashed line shows their average value.

These two equations have been solved by an iterative procedure for the full range of experimental conditions (V_0, i, and electron beam "on" time) used in making H_3O^+ recombination measurements. We find that the low currents used in the high-resolution electron gun produce a maximum temperature increase of the trapped ions of only approximately 20 K, even at the maximum electron-beam "on" time of 1000 sec. The increased loss of ions at this temperature due to evaporation was approximately 0.1%. Thus, data taken with the high-resolution gun are seen to be relatively unaffected by any evaporative loss of ions.

However, the larger electron currents used in making some recombination measurements with the low-resolution electron gun result in a definite heating and subsequent observable cool-down of the ion sample when electrons are removed. There is measurable evaporative loss of ions from this heating only for recombination measurements at electron energies greater than 300 meV. At these higher energies, the decreasing size of the recombination cross section required larger current-time combinations in order to obtain a reasonable recombination loss of ions, and resulted in increased ion heating. Figure 4 shows noise power [product of $N(t)$ and $T(t)$] as a function of time for a recombination measurement made at two different well depths $V_0 = 0.85$ V, and $V_0 = 1.85$ V. Electrons of 0.335 eV at a current of 7×10^{-8} A bombarded the ion sample for 150 sec. The cool-down of the sample at the deeper well depth is evidence that heating of the ions has occurred. One can see that the calculated noise-power signal represented by the solid lines in each case fits the experimental data (dots) quite well, and predicts a maximum ion temperature T_M of 700 K for

$V_0 = 1.85$ V and 560 K when $V_0 = 0.85$ V. The lower ion temperature at the shallower well is due to evaporative cooling which is absent at the deeper well. Note that the initial ion sample temperatures are different, 440 K and 400 K, again due to evaporative effects. The slight difference between initial and final ion temperatures at each well depth is due to the change in ion number $N(t)$, which consequently changes the self-collision time τ_{sc} and thus the evaporative cooling rate. The dashed line in each plot indicates an ideal recombination measurement in the absence of any electron heating. This shows that while the actual measurement at $V_0 = 1.85$ V would be substantially correct, for $V_0 = 0.85$ V the additional evaporative loss of ions would require a correction of approximately 16% to the cross-section measurement. For the low-resolution gun these corrections amounted to a maximum of 18% at energies above 300 meV, except for a single measurement at 1.15 eV made with extremely large current and long "on" time was reduced by a factor of approximately 3 because of the large evaporation correction. Thus we conclude that although electron heating of the ion sample cannot be totally ignored, it is a minor effect in the majority of cases, and one for which corrections can be made.

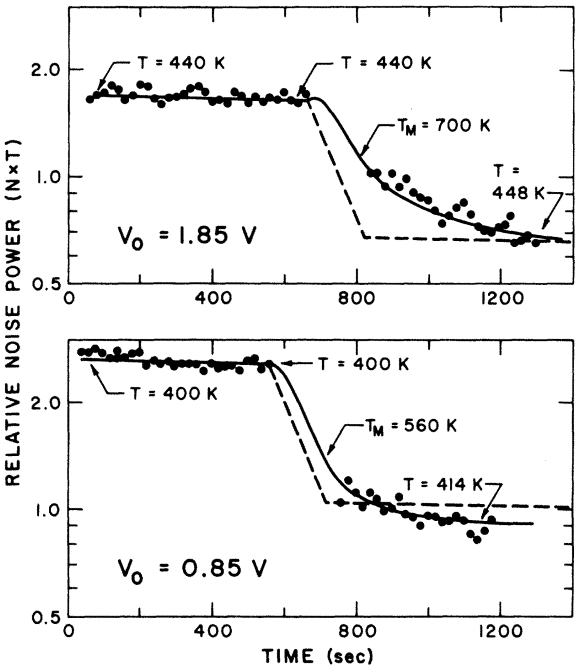

FIG. 4. Recombination cross-section measurements for two different applied potentials, $V_0 = 0.85$ V and $V_0 = 1.85$ V. An electron beam of 0.335 eV energy and 7×10^{-8} A is sent through the ion sample for 150 sec resulting in recombination with and heating of the sample. Representative temperatures are given at various times during the measurement with T_M the maximum temperature obtained. The solid lines are model fits to the measurements using Eqs. (17). The dashed lines are obtained from Eqs. (17) if heating effects are ignored.

Ion loss by dissociation or ionization does not contribute to ξ_e at the energies (0.06–1.15 eV) of this experiment, since the thresholds are significantly above the experimental energies.

Buildup of contributing populations of excited background gas is no problem, since the characteristic formation time of about 10^3 sec is very long compared to the 20-μsec collision period with the walls.

The final contribution to ξ_e in Eq. (16)—that due to excitation of internal modes of the target ions—needs careful attention for each ion species studied. Indeed, this could be an important consideration for, not only the ion-trap technique used here, but also the microwave afterglow technique[51,52] when microwave heating of electrons is employed.

Considering a simple two-level model, in the absence of recombination, an equilibrium population fraction of the excited state will be built up and given by $\tau_D/(\tau_D+\tau_E)$, where τ_D and τ_E are respectively the time constants for deexcitation and excitation of the upper state and include both radiative and collisional effects. This equilibrium is achieved with a time constant given by $\tau_D\tau_E/(\tau_D+\tau_E)$. The collisional time constants for the present experiments are given by $\tau_M = e\mathfrak{A}/i_e\sigma_M$, where subscript M stands for either excitation or deexcitation.

Rotational excitation of ions has recently been considered for both diatomic[53] and symmetric-top[54] molecular ions by Chu and Dalgarno. The particular cases of[53] CH^+ and[54] H_3O^+ were treated. For H_3O^+, it was found that the excitation by interaction with the quadrupole moment is the dominant means of rotational excitation, and that the cross section depends on the particular $(J,K) \rightarrow (J',K')$ transition involved. Typical cross sections are exemplified by the $(3,3) \rightleftharpoons (4,3)$ transitions, and are given by $\sigma_E \approx 29/E$ (10^{-16} cm^2) and $\sigma_D \approx 23/E$ (10^{-16} cm^2), where E is the electron energy in eV. The excitation cross section at the 0.012-eV threshold is thus 2.4×10^{-13} cm^2. If we examine a "worst case" situation, that of low energy and high current, using the low-resolution gun, we find for $E = 0.15$ eV and $i_e = 5\times10^{-8}$ A that $\tau_E = 18$ sec and $\tau_D = 23$ sec. In the absence of radiative decay, this would lead to 44% excited-state population in the two-level model.

[This is still considering the (3, 3) and (4, 3) levels. The (3, 3) level is the most populated H_3O^+ level at 300 K.] Assuming the permanent dipole

moment of H_3O^+ is $0.4ea_0$ as noted in Sec. I, the resulting radiative lifetime for $(4,3)\rightarrow(3,3)$ is about 3.3 sec. This leads to a reduced equilibrium fraction of the excited state in the two-state model of about 14%. Other levels considered have somewhat smaller equilibrium fractions; and since the current-energy combination chosen leads to a "worst case" answer, we have ignored this possible small rotational excitation in subsequent discussion. We rationalize this further by noting that in a crude sense both the bound and repulsive electronic states shift about the same amount with rotational level; so that in the absence of unanticipated resonance effects there should be only a small dependence of the recombination cross section on rotational level.

One may expect rather larger dependences[51] of recombination cross sections upon vibrational levels. Chu[55] has estimated the vibrational excitation cross section for pure vibrational excitation of H_3O^+ (summing over all final rotational states) to be given by

$$\sigma(v\rightarrow v') = \frac{3}{4\pi^2}\frac{\pi}{k_i^2}\,|\langle v|Q_1|v'\rangle|^2 f_{E1}\,, \tag{18}$$

where atomic units are used throughout, Q_1 is the dipole moment expressed as a function of internuclear coordinates, and f_{E1} is a function which varies smoothly for the $0\rightarrow1$ transition from about 64 at the threshold electron energy to 110 at 2 eV. In fact, the matrix element in Eq. (18) depends on the gradient of the dipole moment with internuclear coordinates, and thus requires detailed information to evaluate it. If we factor this quantity out as μ, expressing it in units of ea_0, we can write for $0\rightarrow1$,

$$\sigma(0\rightarrow1) = \mu^2(55+113/E)10^{-16}\ \text{cm}^2\,, \tag{19}$$

where E is in eV. The quantity μ^2 is the same as that appearing in the expression for the radiative lifetime; so this cancels out if we calculate the ratio $\tau_D/(\tau_D+\tau_E)$. For $E=0.17$ eV and $i_e=5\times10^{-8}$ A, we find $\tau_D/(\tau_D+\tau_E)\approx10^{-4}$. This is essentially a "worst case" example, and implies an equilibrium population fraction of excited state in the two-state model of less than 0.01%. The effect of vibrational excitation on the recombination measurements is thus assessed to be negligible.

Rotational- and vibrational-state excitation by electron impact may be a problem in any type of recombination experiment for which the electron temperature is different from that of the ions. For some other experimental techniques operating densities are several orders of magnitude higher than in this experiment ($\rho\simeq1\times10^6/\text{cm}^3$), and thus collisional relaxation of excited ions may help to reduce populations of excited levels. The effect of collisional relaxation, excited-state lifetime, measurement time, and excitation and deexcitation times should be considered and evaluated for each specie studied.

Concluding the discussion of ξ_e which appeared in Eq. (16), we have considered the possible contributions to ξ_e and find most of them to be negligible for these recombination measurements on H_3O^+. The main contributor to ξ_e appears to be electron heating of the ion sample which becomes important under certain operating conditions. Then Eq. (3) is not a good approximation and a more careful extraction of the cross-section value from the measurement as illustrated in Fig. 4 is necessary.

One further possible systematic effect deserves discussion at this point. If, after formation, the ions redistribute in space in such a way that a portion of the ions can be bombarded by electrons and a portion cannot, then the ion numbers properly entering into Eq. (3) are not the ones observed. Thus, there could be a "hole burned" in the ion sample, eliminating all accessible ions, but leaving a sizeable ion signal. However, by making several successive "kills" with the same ion sample and verifying the constancy of the cross section this effect was shown to be negligible. Similarly, it was easy to verify that in a trapped sample all ions could be "killed" by recombination, and were thus all accessible to the electron beam.

D. Measurement of overlap $\mathcal{A}$

The geometric overlap $\mathcal{A}$ appearing in Eqs. (3), (4), and (16) is the only quantity not measured in each data run. In principle, it is possible to measure the radial distributions $\xi_i(r)$ and $\mathcal{F}(r)$ appearing in Eq. (4), but this was not done. Instead we used an indirect method which was described earlier.[20] Essentially in this method the cross section for recombination of electrons and O_2^+ was measured, reducing the data according to Eq. (3) and leaving the unknown factor $\mathcal{A}$ multiplying the results. Rate coefficients were then calculated according to Eq. (2), with the results again having the factor $\mathcal{A}$ as a multiplier. These rate coefficients were then equated to measured rate coefficients, and the equation solved for $\mathcal{A}$. The equality was set at a temperature (2000 K) where there is negligible influence of the cross section below and above those energies at which measurements were made. Oxygen was chosen since there are numerous measurements which agree very well in this temperature range.

In order to use the value of $\mathcal{A}$ determined for O_2^+ for other ion species, we must insure that $\mathcal{A}$ is relatively insensitive to the cyclotron radius of the ion, which of course may change with ion

species. Recombination measurements at 0.335 eV for H_3O^+ were found to be independent of magnetic field strength, and thus cyclotron radius, to within the uncertainty of our measurements for fields ranging from 0.675 to 1.175 T. For equal radial kinetic energies, the cyclotron radius for an H_3O^+ ion and an O_2^+ ion will be equal for magnetic fields of 0.905 and 1.175 T, respectively. Thus we conclude that α is independent of cyclotron radius over the magnetic field range given above, and have used the overlap value measured for O_2^+ at 1.175 T in determining the cross-section results presented in Sec. III for H_3O^+ (for which the data were also taken at a field of 1.175 T).

The overlaps were rechecked for the present measurement by remeasuring cross sections[20] for NO^+.

III. RESULTS AND DISCUSSION

A. Recombination cross-section measurements

Recombination cross-section data for the hydronium ion taken with the high- and low-resolution electron guns are shown by dots in Figs. 5(a) and 5(b). Also shown are representative uncertainties in these measurements at several data points. The measured cross sections should be recognized as resulting from physical convolutions of each electron energy distribution with the true cross section. One thus expects a difference between measurements obtained using the high- and low-resolution electron guns at energies where the variations in the true cross section are rapid compared to the width of the electron energy distribution. This accounts for the large differences

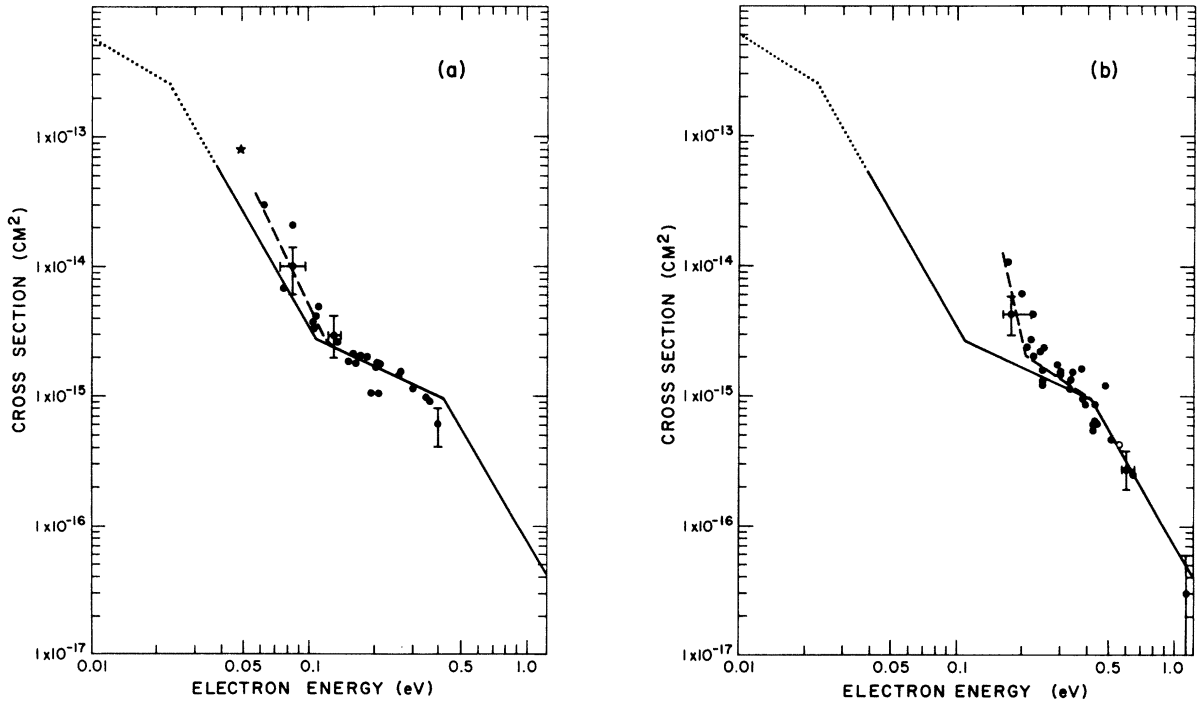

FIG. 5. Electron-H_3O^+ recombination cross section vs electron energy, taken with the narrow electron energy distribution of the high-resolution electron gun (a), and with the wide energy distribution of the low-resolution electron gun (b). In both (a) and (b) the actual cross-section data are indicated by the points, the solid line represents the deduced cross section, the dashed lines represent a convolution of the deduced cross section with the respective electron energy distributions. The dotted lines represent an extension of the deduced cross section, made to be consistent with the present data, the rate-coefficient measurement of Leu *et al.* (Ref. 10), and with threshold behavior of recombination cross sections (Refs. 56, 57). The open circle in (b) at 565 meV represents the average value of the nine measurements shown in Fig. 2. The star represents the average cross-section value obtained from the rate-coefficient measurement of Leu *et al.* (Ref. 10). Representative uncertainties are indicated at selected data points.

between measured values in Fig. 5(a) and 5(b) for $E \lesssim 0.25$ eV.

In an attempt to arrive at a closer estimate of the true cross section, various trial functions were convoluted with the energy distributions shown in Fig. 2. By successive adjustments, a function was arrived at which gives convoluted values consistent with the measured values. Thus, convoluting the solid curve in Fig. 5 with the energy distributions of Fig. 2 gives the dashed curves through the points in Fig. 5. Though there is, of course, no uniqueness statement possible, the close agreement between both dashed curves with both sets of measurements leads us to believe that the solid curve is a close estimate of the cross section. The solid curve is expressed by

$$\sigma = 4.6\times10^{-18}E^{-2.9\pm0.4}\ \text{cm}^2,\quad 38 < E \leq 110\ \text{meV},$$
$$\sigma = 4.8\times10^{-16}E^{-0.79\pm0.1}\ \text{cm}^2,\quad 110 < E \leq 420\ \text{meV},$$
$$\sigma = 7.5\times10^{-17}E^{-2.9\pm0.2}\ \text{cm}^2,\quad E > 420\ \text{meV}. \quad (20)$$

The estimated uncertainty in the overlap factors[20] $\mathcal{C}$ and $\mathcal{C}'$ for the two electron guns is approximately ±30%, and the standard deviation of a cross-section measurement is approximately ±35%. For the low-resolution gun the electron energy is estimated to be accurate to +45 and −10 meV (limited by the uncertainty in the energy in the transverse motion); while for the high-resolution electron gun the uncertainty in the electron energy is ±10 meV.

The cross-section measurements in this experiment do not extend to low enough energies to give much information about the cross section below 60 meV. Thus, the estimate shown as a dotted extension of the solid curve in Fig. 5 has been arrived at using additional considerations discussed below in Sec. III B. In performing the convolutions discussed above to get the dashed curves of Fig. 5, the dotted extensions were included in the integrations, though the dashed-curve results were quite insensitive to this portion of the estimated cross section.

These are the first measurements of the recombination cross section for H_3O^+ ions. There are no other direct experimental measurements or theoretical predictions available with which to compare these results. Several experimental groups have measured the rate coefficient for H_3O^+ recombination, which can be converted into an apparent cross section by dividing by the average electron velocity $\bar{v}$. This has been done for the measurement of Leu *et al.*[10] and is shown by the star in Fig. 5(a). It is interesting to note that the star point would be in good agreement with an extension of the dashed line indicating our direct measurement of the cross section, which is also larger than the deduced cross section due to the convolution effects discussed earlier. In comparing the present cross-section results with rate-coefficient measurements, it is probably more appropriate to calculate rates from the measured cross sections and compare, as is done in the next section.

B. Rate coefficient calculations and comparisons

In order to use Eq. (2) to calculate rate coefficients for recombination, the cross-section results must be extended below 38 meV. It is reasonable to suppose that the same slope as found for $38 < E < 110$ meV may continue for some distance below 38 meV. However, the threshold laws of Wigner[56] and analysis of the recombination process by Bardsley[57] show that the cross section will eventually go as E^{-1} as the energy approaches the threshold (zero?) energy. Thus, we have assumed the cross section to be given by

$$\sigma = 6.0\times10^{-15}E^{-1}\ \text{cm}^2,\quad 0 < E \leq E_T,$$
$$\sigma = 4.6\times10^{-18}E^{-2.9\pm0.4}\ \text{cm}^2,\quad E_T < E < 38\ \text{meV}. \quad (21)$$

The cross sections given by Eqs. (20) and (21) were used in Eq. (2) to calculate the rate coefficient α. The value of E_T in Eq. (21) was chosen to be 23 meV by adjusting it until the calculated value of α agreed with the measured rate coefficient of Leu, Biondi, and Johnsen[10] at 540 K. The calculated rate coefficient is quite sensitive to the value of E_T. For instance, if one forces the cross section to go as E^{-1} at energies of 15 meV and lower, the calculated rate coefficient α at $T = 540$ K is 1.7×10^{-6} cm^3 sec^{-1}; for $E_T = 35$ meV, $\alpha = 5.6\times10^{-7}$ cm^3 sec^{-1} at the same temperature.

With E_T thus fixed at 23 meV, Eqs. (2), (20), and (21) were used to calculate rate coefficients (assuming a Maxwellian velocity distribution for the electrons) for $10 < T < 10^5$ K. The resulting rate coefficients are represented by the solid curve in Fig. 6. The dotted and dot-dashed curves represent calculated values when the uncertainty variations given in Eqs. (20) and (21) are applied to the cross section; except that at temperatures above 10^4 K most of the difference between the three curves arises from different ways of extrapolating the cross section past 1.15 eV (the highest energy at which measurements were made). The high-temperature portion of the dotted curve arises by assuming the cross section has a constant value of 1.0×10^{-16} cm^2 for $E \geq 1.15$ eV; the dot-dashed curve results when it is assumed that the cross section is zero for $E \geq 1.15$ eV; and the solid curve represents the calculated values if it is assumed the cross section continues to decrease as $E^{-2.9}$ for $E \geq 1.15$ eV.

The power dependence of the rate coefficient upon temperature is indicated with arrows at four places along the curve in Fig. 6. It is shown to vary from $T_e^{-0.5}$ below 100 K to $T_e^{-1.43}$ near 10^5 K. One can show by using a step function model for the cross section in Eq. (2) that the rate coefficient can never decrease faster than $T_e^{-3/2}$ for a Maxwellian electron velocity distribution, and the present results are asymptotically approaching this limiting behavior.

Also shown in Fig. 6 are results from the microwave afterglow experiment of Leu, Biondi, and Johnsen,[10] the glow discharge measurement of Lindinger,[19] the shock tube experiments of Wilson and Evans,[18] and the flame study measurement of Green and Sugden.[2] There are results from a number of other flame studies which, for clarity's sake, have not been included in Fig. 6. These rate coefficients are all for temperatures near 2000–2500 K and have values (units 10^{-7} cm^3 sec^{-1}) 2.5,[11] 0.5,[12] 2.0,[13] 2.2,[14] 2.4,[15] 4.0,[16] and 4.7.[17]

We note that for all the rate coefficient measurements except that of Lindinger, the ion temperature is presumably equal to the electron temperature. However, for the present measurements the ion temperature is fixed at $T_i \approx 400$ K, and for Lindinger's experiment $T_i \approx 300$ K. There is thus a certain inconsistency in comparing these results with our calculated rate coefficients. We have already noted in Sec. II C that it is not unreasonable to have a significant dependence of recombination cross section upon vibrational level. Since the first excited vibrational level of H_3O^+ lies about 0.14 eV above the ground level, one may expect greater than 20% populations of this excited level at ion temperatures above 1000 K. The agreement of the present results and those of Lindinger with the measurements having high T_i may indicate for H_3O^+ there is not a strong dependence of the recombination cross section upon vibrational level.

The rate coefficients calculated from our cross-section measurements are in general agreement with the direct rate coefficient measurements. The structure shown in the recombination cross section probably indicates the contribution of more than one molecular state to the recombination process. However, more detailed knowledge of the potential surfaces of H_3O^+ and H_3O is necessary before further interpretation of the observed cross section structure is possible.

The distinction between our cross-section measurements given by dots in Fig. 5 and the deduced cross section given by Eqs. (20) and (21) is again emphasized. The forms given in Eqs. (20) and (21) have been chosen to be consistent with (i) our cross-section measurements using the high-resolution electron gun, (ii) our cross-section measurements using the low-resolution gun, (iii) Leu, Biondi, and Johnsen's[10] rate-coefficient measurement at 540 K, and (iv) threshold laws[56,57] for the capture process.

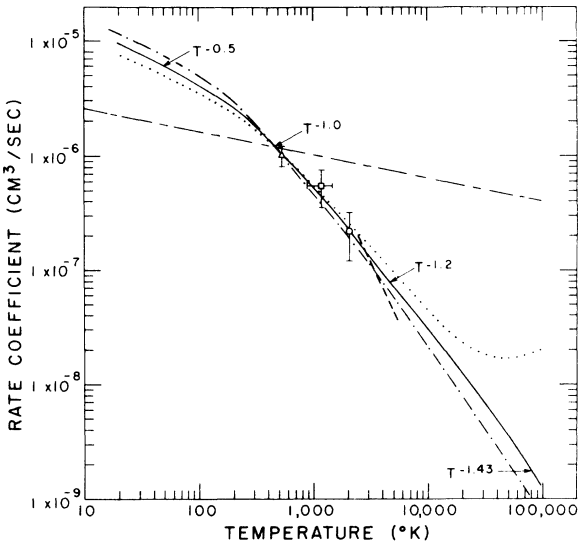

FIG. 6. Electron-H_3O^+ recombination rate coefficient as a function of electron temperature T_e. The solid curve is calculated from our deduced cross-section data (the solid lines with dotted extension in Fig. 5) by using Eq. (2) in conjunction with a Maxwellian electron velocity distribution. The points represent the measurements of Leu *et al.* (Ref. 10), △; Lindinger (Ref. 19), □; and Green and Sugden (Ref. 2), ○. The dashed line represents the data of Wilson and Evans (Ref. 18). The dotted and dot-dashed curves result when uncertainties in the cross section and various methods of extrapolating the cross section to $E > 1.15$ eV are introduced as discussed in Sec. III B. The short-long dashed curve represents the rate-coefficient estimate given in Ref. 58. The temperature dependence of the recombination coefficient is indicated at four temperatures. For the data of Refs. 2, 10, and 18 the electron and ion temperatures are equal.

ACKNOWLEDGMENTS

The authors are grateful for helpful discussions with J. N. Bardsley, J. Whealton, M. A. Biondi, A. V. Phelps, and H. H. Michels. They are especially grateful to S. I. Chu for calculating rotational and vibrational excitation cross sections for H_3O^+.

*Work supported in part by the Aeronomy Program of the National Science Foundation through Grant No. GA-35065.

†Present address: Time and Frequency Division, National Bureau of Standards, Boulder, Colo. 80302.

‡Staff Member, Laboratory Astrophysics Division, National Bureau of Standards.

[1]R. S. Narcisi, Space Res. 7, 186 (1967).

[2]J. A. Green and T. M. Sugden, in *Ninth Symposium on Combustion* (Combustion Institute, Pittsburgh, Pa., 1963), p. 607.

[3]L. J. Denes and J. J. Lowke, Appl. Phys. Lett. 23, 130 (1973).

[4]A. V. Phelps (private communication, 1973).

[5]E. Herbst and W. Klemperer, Astrophys. J. 185, 505 (1973).

[6]H. Lischka and V. Dyczmons, Chem. Phys. Lett. 23, 167 (1973).

[7]J. W. Moskowitz and M. C. Harrison, J. Chem. Phys. 43, 3550 (1965).

[8]G. Herzberg, *Infrared and Raman Spectra of Polyatomic Molecules* (Van Nostrand, Princeton, 1962), p. 252.

[9]C. C. Ferriso and D. F. Hornig, J. Chem. Phys. 23, 1464 (1955).

[10]M. T. Leu, M. A. Biondi, and R. Johnsen, Phys. Rev. A 7, 292 (1973).

[11]I. R. King, J. Chem. Phys. 27, 817 (1957).

[12]I. R. King, J. Chem. Phys. 35, 380 (1961).

[13]H. F. Calcote, *Eighth International Symposium on Combustion* (Williams and Wilkins, Baltimore, 1962), p. 184.

[14]E. S. Semenov and A. S. Sokolik, Zh. Tekh. Fiz. 32, 1074 (1962) [Sov. Phys.-Tech. Phys. 7, 788 (1962)].

[15]H. F. Calcote, S. C. Kurzius, and W. J. Miller, in *Tenth International Symposium on Combustion* (Combustion Institute, Pittsburgh, 1965), p. 605.

[16]R. Kelly and P. J. Padley, Trans. Faraday Soc. 66, 1127 (1970).

[17]A. N. Hayhurst and N. R. Telford, Nature Phys. Sci. 235, 114 (1972).

[18]L. N. Wilson and E. W. Evans, J. Chem. Phys. 46, 859 (1967).

[19]W. Lindinger, Phys. Rev. A 7, 328 (1973).

[20]F. L. Walls and G. H. Dunn, J. Geophys. Res. 79, 1911 (1974).

[21]F. M. Penning, Physica 3, 873 (1936).

[22]J. R. Pierce, *Theory and Design of Electron Beams* (Van Nostrand, Princeton, 1954), 2nd ed., p. 40.

[23]J. Byrne and P. S. Farago, Proc. Phys. Soc. (Lond.) 86, 801 (1965).

[24]G. Gräff and E. Klempt, Z. Naturforsch. 22a, 1960 (1967).

[25]G. Gräff, F. G. Major, R. W. H. Roeder, and G. Werth, Phys. Rev. Lett. 21, 340 (1968).

[26]H. G. Dehmelt and F. L. Walls, Phys. Rev. Lett. 21, 127 (1968).

[27]H. G. Dehmelt, in *Advances in Atomic and Molecular Physics*, edited by D. R. Bates and I. Esterman (Academic, New York, 1967), Vol. 3, p. 53; Vol. 5 (1969), p. 109.

[28]G. Gräff, E. Klempt, and G. Werth, Z. Phys. 222, 201 (1969).

[29]D. A. Church and H. G. Dehmelt, J. Appl. Phys. 40, 3421 (1969).

[30]F. L. Walls, Ph.D. thesis (University of Washington, Seattle, 1970) (unpublished), available through University Microfilms, Inc., Ann Arbor, Mich.

[31]D. A. Church and B. Mokri, Z. Phys. 244, 6 (1971).

[32]M. H. Prior and H. A. Shugart, Phys. Rev. Lett. 27, 902 (1971).

[33]M. H. Prior, Phys. Rev. Lett. 29, 611 (1972).

[34]D. Wineland, P. Ekstrom, and H. Dehmelt, Phys. Rev. Lett. 31, 1279 (1973).

[35]F. L. Walls and T. S. Stein, Phys. Rev. Lett. 31, 975 (1973).

[36](a) H. Dehmelt, P. Ekstrom, and D. Wineland, Bull. Am. Phys. Soc. 19, 572 (1974); H. Dehmelt, P. Ekstrom, D. Wineland, and R. Van Dyck, Bull. Am. Phys. Soc. 19, 572 (1974); D. Wineland and H. Dehmelt, Bull. Am. Phys. Soc. 19, 642 (1974); H. Dehmelt, R. Van Dyck, P. Ekstrom, and D. Wineland, Bull. Am. Phys. Soc. 19, 643 (1974); (b) D. Wineland and H. Dehmelt, in *Proceedings of the Fourth International Conference on Atomic Physics, Abstracts of Contributed Papers, Heidelberg, July, 1974*, edited by J. Kowalski and H. G. Weber (Heidelberg U. P., 1974), p. 89.

[37]F. L. Walls and G. H. Dunn, Phys. Today 27 (No. 8), 30 (1974).

[38]E. N. Fortson and M. D. McGuire, in Ref. 36(b), p. 425.

[39]D. J. Wineland and H. G. Dehmelt (private communication, 1974).

[40]L. Spitzer, *Physics of Fully Ionized Gases* (Interscience, New York, 1962), 2nd ed., Chap. 5.

[41]I. A. Fleming, R. J. Tunnicliffe, and J. A. Rees, J. Phys. B 2, 780 (1969).

[42]C. E. Young and W. E. Falconer, J. Chem. Phys. 57, 918 (1972).

[43]S. Dushman, *Scientific Foundations of Vacuum Technique* (Wiley, New York, 1966), p. 49.

[44]V. L. Tal'roze and E. L. Frankevich, Zh. Fiz. Khim. 34, 2709 (1960) [Russ. J. Phys. Chem. 34, 1275 (1960)].

[45]F. C. Fehsenfeld, A. L. Schmeltekopf, and E. E. Ferguson, J. Chem. Phys. 46, 2802 (1967).

[46]W. T. Huntress, Jr., R. F. Pinizzotto, Jr., and J. B. Laudenslager, J. Am. Chem. Soc. 95, 4107 (1973).

[47]A. Stamatović and G. J. Schulz, Rev. Sci. Instr. 41, 423 (1970).

[48]J. W. McGowan, Rev. Sci. Instr. 38, 285 (1967).

[49]T. D. Roberts and D. S. Burch, Rev. Sci. Instr. 35, 1067 (1964).

[50]P. O. Taylor, K. T. Dolder, W. E.Kauppila, and G. H. Dunn, Rev. Sci. Instr. 45, 538 (1974).

[51]J. N. Bardsley and M. A. Biondi, in *Advances in Atomic and Molecular Physics*, edited by D. R. Bates and I. Esterman (Academic, New York, 1970), Vol. 6, pp. 1–57.

[52]F. J. Mehr and M. A. Biondi, Phys. Rev. 181, 264 (1969).

[53]S. I. Chu and A. Dalgarno, Phys. Rev. A 10, 788 (1974); 12, 725(E) (1975).

[54]S. I. Chu, Phys. Rev. A 12, 396 (1975).

[55]S. I. Chu (private communication, 1974).

[56]E. P. Wigner, Phys. Rev. 73, 1002 (1948).

[57]J. N. Bardsley, Phys. Rev. A 2, 1359 (1970).

[58]M. A. Biondi, in Defense Nuclear Agency Reaction Rate Handbook, pp. 16–17, 16–27, Document No. DNA 1948H (Revised Chapter August 1971) (unpublished).